processes

MDPI

Article

Dynamic Mechanical and Failure Properties of Grouted Fractured Rock Based on Nano-Grouting Material

Yuhao Jin [1,2], Shuo Yang [1,2,*], Hui Guo [3], Lijun Han [4], Pengcheng Huang [1,*], Miao Chen [5], Hao Shan [1], Lanying Huang [1], Shanjie Su [1], Shengcheng Wang [1], Peitao Qiu [1], Xiaoxi Bi [1] and Zu-an Liu [1]

[1] School of Civil Engineering, Xuzhou University of Technology, Xuzhou 221018, China
[2] School of Mines, China University of Mining and Technology, Xuzhou 221116, China
[3] Xuzhou Science and Technology Information Institute, Xuzhou 221008, China
[4] State Key Laboratory of Intelligent Construction and Healthy Operation and Maintenance of Deep Underground Engineering, China University of Mining and Technology, Xuzhou 221116, China
[5] College of Energy and Mining Engineering, Shandong University of Science and Technology, Qingdao 266590, China
* Correspondence: yangshuo@xzit.edu.cn (S.Y.); 12241@xzit.edu.cn (P.H.)

Abstract: Fractured rock masses are extremely common in geological engineering. In order to improve the stability of surrounding rock under dynamic conditions, new grouting materials and their reinforcement characteristics were studied. In this paper, split Hopkinson pressure bar (SHPB) tests were employed to analyze the dynamic mechanical and failure characteristics of grouted fractured rock with nano-grouting material (nano-grouted fractured rock). Simultaneously, high-speed camera tests were utilized to examine the macroscopic dynamic deformation and failure processes. The following was found: (1) Under a relatively low impact air pressure of 0.1 MPa, the mechanical properties of nano-grouted fractured rock are considerably better than those of traditional cement-based grouted rock. However, when the impact air pressure is increased to 0.3 MPa, the superiority of nano-grouting material diminishes, the possible cause of which is explained from the microscopic point of view. This means the nano-grouting material is more suitable for low-engineering-disturbance conditions (e.g., shield construction). (2) Both for the nano- and superfine cement grouting material, the impact fractures initially emerge at the two ends of the original grouted fracture and form a pair of parallel lines. (3) In comparison with 0.1 MPa, the impact pressure of 0.3 MPa leads to more severe damage to the rock specimen. These findings contribute to a deeper understanding of the behavior of nano-grouted fractured rock under dynamic loading and provide valuable insights for relevant engineering applications in the field of rock mechanics and grouting technology.

Keywords: geological engineering; mechanical properties; nano-grouting material; grouted fractured rock; split Hopkinson pressure bar tests

check for updates

Academic Editors: Guanghui Zhao, Tingzhuang Han, Tao Meng, Gan Feng and Reza Taherdangkoo

Received: 6 February 2025
Revised: 2 March 2025
Accepted: 3 March 2025
Published: 6 March 2025

Citation: Jin, Y.; Yang, S.; Guo, H.; Han, L.; Huang, P.; Chen, M.; Shan, H.; Huang, L.; Su, S.; Wang, S.; et al. Dynamic Mechanical and Failure Properties of Grouted Fractured Rock Based on Nano-Grouting Material. *Processes* **2025**, *13*, 765. https://doi.org/10.3390/pr13030765

Copyright: © 2025 by the authors. Licensee MDPI, Basel, Switzerland. This article is an open access article distributed under the terms and conditions of the Creative Commons Attribution (CC BY) license (https://creativecommons.org/licenses/by/4.0/).

1. Introduction

In the field of tunnel engineering (such as tunnel excavation and coal mining engineering), fractured rock masses are extremely common geological conditions [1–3]. Due to the complex tectonic movements, long-term weathering effects, and erosion influence of groundwater, intricate fracture networks form within the rock masses [4,5]. The existence of fractures reduces the bearing capacity of rock masses and brings hidden trouble to geotechnical engineering [6]. Figure 1 shows the fractured rock masses.



Figure 1. Fractured rock masses.

Dynamic load refers to the load that changes with time, which is more common in geotechnical engineering. Under dynamic loading, fractured rock masses undergo rapid degradation in structural integrity and mechanical strength, critically jeopardizing both the construction and operational safety of underground engineering projects [7]. Dynamic loads generated by blasting operations cause the fractured rock in tunnels surrounding rock to endure intense vibrations and impacts, and enormous stress concentrations occur at the tips of fractures [8,9]. As the continuity of the rock is disrupted by fractures, stress cannot be effectively transmitted and dispersed, resulting in the cracking, spalling, or even massive collapses of the rock masses [10,11]. This will not only cause serious damage to the tunnel structure but may also block traffic routes, posing great difficulties for rescue and emergency work.

To effectively address the threats posed by fractured rock masses to tunnel projects, the grouting reinforcement method is widely adopted: by injecting grouting materials into fractured rock, the grout fills and solidifies in the fractures, integrating with the rock masses to form a hole, thereby significantly enhancing the mechanical strength of the fractured rock masses [12–16]. Grouting materials are essential for grouting reinforcement engineering. In tunnel excavation and coal mining engineering, grouting materials are categorized into cement-based and chemical grouts [17–19]. Cement-based grouts, primarily composed of ordinary Portland cement (OPC) with additives like clay or fly ash, offer high compressive strength and durability, making them suitable for reinforcing fractured rock masses. However, their limitations include poor stability, coarse particle size, and limited penetration into fine fractures. Chemical grouts, such as polyurethane and epoxy resins, exhibit superior injectability and rapid curing, ideal for tight schedules and micro-fracture sealing. Grouting material selection depends on geological conditions, with cement-based grouts preferred for permanent structures and chemical grouts for urgent water sealing.

Grouting reinforcement can improve the mechanical indices of the rock, such as shear resistance, compressive strength, and tensile strength, and improve the self-supporting ability of the surrounding rocks, providing a reliable safeguard for the stability of the tunnel [20,21]. However, although scholars have carried out a large amount of research work on the mechanical properties of grouted rock, this research has mainly been on the static loading conditions. The research contents mostly involve the strength characteristics, deformation laws, and material durability. For example, Jin et al. studied the mechanical behaviors of grouted crushed coal rocks under uniaxial compression, which showed that the uniaxial compression strength of grouted specimens decreased with the decrease in the crushed degrees of coal rock at a constant solidified grout strength [22]; Le et al. performed a series of pull-off and direct shear tests to obtain the tensile strength, peak shear strength, and residual shear strength of the foliation in different metamorphic rocks, which found that the tensile and shear strengths of the schists were higher than those of slate [23]. These research results have provided an important theoretical base and technical guidance for the

design and construction of grouting in tunnel engineering under static loading conditions, ensuring the safety and stability of tunnels to a certain extent.

Nevertheless, in actual tunnel engineering, dynamic loading cannot be ignored [24,25]. Compared with static loading, there are obvious deficiencies in the mechanical and failure characteristics of grouted rock under dynamic loading [26,27]. Currently, research in this regard is relatively scarce, resulting in difficulties in accurately predicting the mechanical behaviors and failure modes of grouted rock when facing dynamic loading conditions such as earthquake, blasting, and excavation disturbance, not providing precise theoretical support for the seismic design and blasting safety control of tunnel engineering.

Meanwhile, nano-materials exhibit outstanding physical and chemical properties due to their unique nano-scale effects, such as a high specific surface area, small size effect, surface and interface effects, and quantum size effect [28]. They have been widely applied and deeply studied in numerous fields such as electronics, energy, and biomedicine [29,30]. Moreover, nano-materials have shown remarkable beneficial effects on grouting reinforcement. Their ultra-small particle size allows for excellent dispersion in grout, improving the fluidity and penetration ability of the grout. For instance, nano-particles can fill the micro-pores in the rock, enhancing the compactness and mechanical properties of the grouted structure and cemented rockfill [31,32]. The nano-silica sol-based composite grouting material has good sealing and reinforcing effects in rock [33]. As for a concrete example of the application of nano-grouting material, this research studied the grout containing nano-silica sol to reinforce the fractured rock mass [34]. The results showed the peak strength of the sandstone specimens reinforced by the micro–nano-siliceous grout increased by 16.49% compared to those of the sandstones reinforced by the ordinary grout, and the elastic energy accumulated by the former was higher. Finally, based on the 1790 ventilation roadway of the Shiyakou coal mine, the effectiveness and feasibility of the micro–nano-siliceous grout for reinforcing underground engineering surrounding rocks were verified using numerical simulation: for example, the deformation and extent of the plastic zone were significantly reduced than using ordinary grout.

Although there were some studies related to the mechanical properties of cemented and nano-grouted structures, research on the dynamic mechanics of nano-grouted fractured rock in tunnels is still in its infancy. Key issues such as the stress–strain relationship, a macroscopic failure characteristic of nano-grouted fractured rock, have not been deeply investigated.

In this paper, the dynamic mechanical properties of nano-grouted fractured rock were obtained by split Hopkinson pressure bar (SHPB) tests; the macroscopic dynamic deformation and failure processes were analyzed by high-speed camera tests. These results provide references for the grouting design and construction of tunnel engineering under dynamic loading environments.

2. Experimental Materials and Methods

2.1. Preparation of Grouting Material

Preparing nano-grouting material with the mixing ratio of water–superfine cement–nano-material = 24:40:1, in which the nano-material is aqueous CNT dispersion liquid (Figure 2).

The dispersant is deionized water, and the dispersion method is sand mill dispersion. After the dispersion of CNTs, the suspension presents a uniform and stable state without obvious agglomeration or precipitation. Some key parameters of the aqueous CNT dispersion liquid are shown in Table 1.

In order to compare the traditional grouting material, the superfine cement grout without nano-material was prepared, and the water–cement ratio was unchanged.



(**a**) CNT dispersion liquid



(**b**) Material mixing



(**c**) Stir

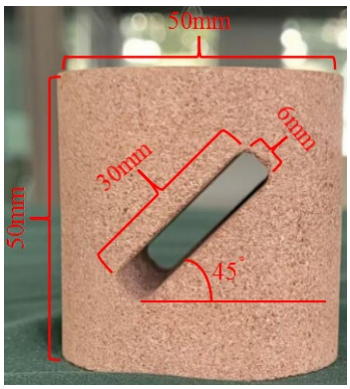
Figure 2. Preparation of nano-grouting material.

Table 1. Some key parameters of the aqueous CNT dispersion liquid.

Test Project	Unit	Specifications
Viscosity	mPas	5000–8000
Solid content of CNTs	%	15
Fineness	nm	30–50

2.2. Preparation of Grouted Fractured Rock Specimens

The initial rock specimen selected was a single fractured red cylindrical sandstone, with a diameter and height of 50 mm (Figure 3a). According to the size of the fractured rock specimen in our study, fracture width classification standard, and common fracture width range of deep rock masses, the fracture width was selected as 6 mm.



(**a**) Single fractured red sandstone



(**b**) Fracture sealing

Figure 3. Fractured rock specimen and sealing treatment.

To prevent any leakage of the grout injected into the fracture, butyl waterproof tape was used to seal one side of the fracture (Figure 3b), and the other side of the fracture was used as a grout inlet. Using the small syringe, the prepared nano-grout and superfine cement grout were injected into the specimen fractures separately (Figure 4). It is noteworthy that due to the fracture not being planar but possessing a certain degree of curvature, during the initial grouting, a small amount of grout was lost along the lower end of the fracture. Consequently, a method of supplementary grouting needed to be employed to fill the fracture completely. At last, these fractured specimens were cured at room temperature for 7 days to form grouted specimens.

2.3. Hopkinson Experimental System and Experimental Scheme

The schematic diagram and experimental system of Hopkinson (developed by the Xuzhou University of Technology) are shown in Figure 5a,b. The size of the launching tube

in the Hopkinson experimental system is 100 mm in diameter and 3000 mm in length; the size of the incident bar is 100 mm in diameter and 5500 mm in length; and the size of the transmission bar is 100 mm in diameter and 4000 mm in length. The rod system is made of 60Si2CrA steel. Signals are collected in real time through the ultra-dynamic strain indicator and the strain gauges on the incident and transmission bars. In addition, the i-SPEED 508 high-speed camera (iX Cameras Ltd., UK) is used to capture the whole process of dynamic failure for grouted rock specimen.

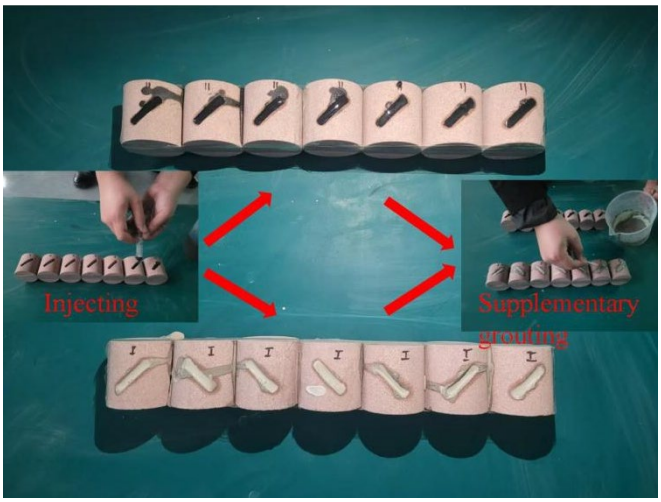
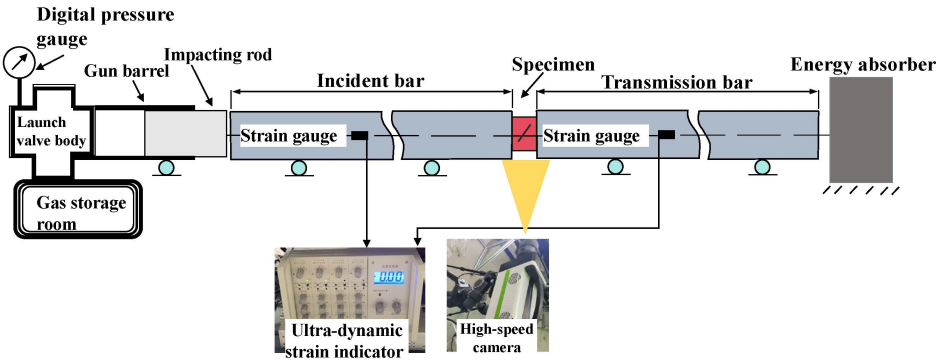
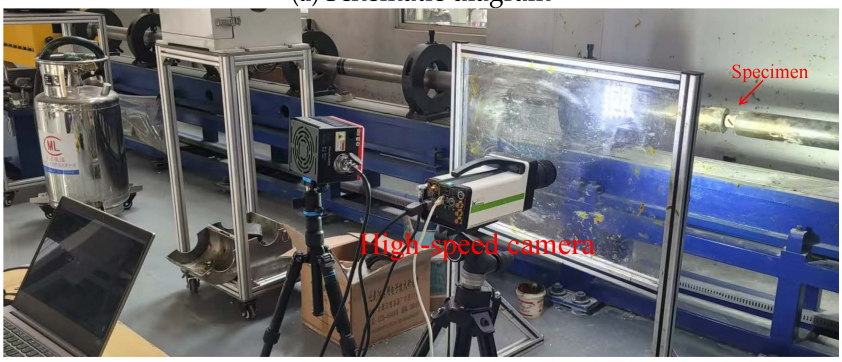


Figure 4. Production of grouted fractured specimens.



(**a**) Schematic diagram



(**b**) Picture of experimental system

Figure 5. Hopkinson experimental system with high-speed camera.

For the nano-grouting and superfine cement grouting fractured sandstone specimens after curing, dynamic impact experiments were carried out under the conditions of different impact air pressures (0.1 and 0.3 MPa), which are in strict accordance with procedures.

3. Dynamic Mechanical and Macroscopic Failure Characteristics of Grouted Fractured Rock

3.1. Dynamic Mechanical Characteristic

Figure 6a,b show the dynamic stress–strain curves of grouted fractured specimens with nano- and superfine cement grouting materials under different impact air pressure conditions. Figure 7 presents the dynamic peak strength of the grouted specimens under different impact air pressures and grouting materials. It can be observed from the figures that when the impact air pressure is relatively low (0.1 Mpa), the nano-grouted fractured rock exhibits more superior mechanical properties compared to the traditional cement-based grouted rock, with its dynamic peak strength increasing by 62.15%. However, as the impact air pressure rises, this trend is reversed. In contrast to the cement-based grouted rock, the dynamic peak strength of the nano-grouted fractured rock decreases by 56.24%. This indicates that the nano-grouting material has a better grouting effect under lower-strain-rate conditions.

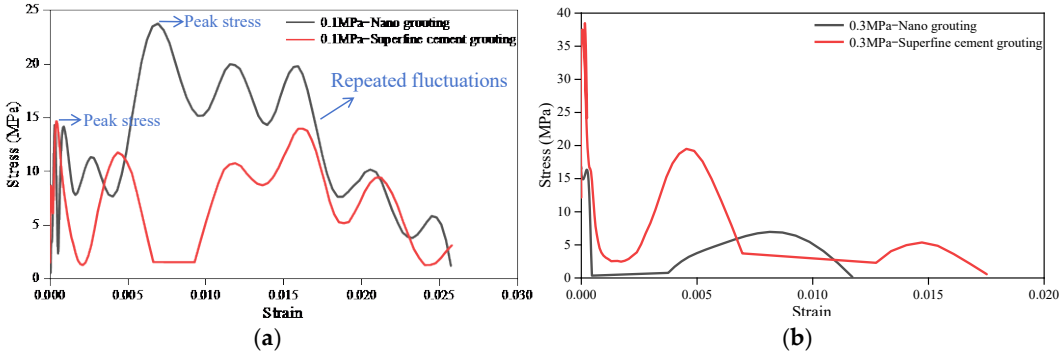


Figure 6. Dynamic stress–strain curves of grouted fractured rock specimens with impact air pressure of (**a**) 0.1 and (**b**) 0.3 MPa.

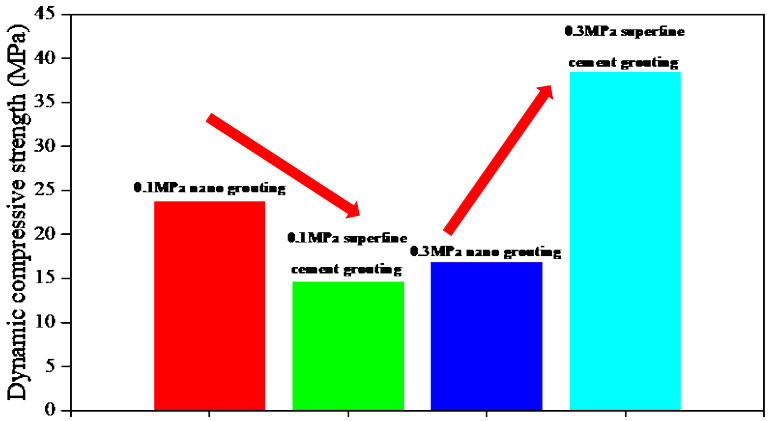


Figure 7. Dynamic peak strength of grouted fractured rock specimens.

Moreover, the impact pressure of 0.1 MPa is taken as an example to analyze the deformation and damage of the specimen: the stress–strain curves demonstrate the repeated increases and decreases in stress, subsequently entering the phase of repeated fluctuations.The slopes of curve display long-term and reciprocating changes. This phenomenon means the grouted fractured rock suffered severe cracking (large deformations occur) and damage after being impacted, and further deformation and damage occur as the impact continues.

To further explain the possible reason why the effect of nano-grouting material is not as good as that of superfine cement grouting material under the impact air pressure of

0.3 MPa, SEM tests were carried out to try to explain this phenomenon from a microscopic perspective. As can be seen in Figure 8, nano-grouting material has more pores (red circular and oval marks in the figure), which reduces the reinforcement characteristics of the grouting material to a certain extent: the initiation and development of micro-pores in microstructure significantly affect the dynamic properties of grouted sandstone. First of all, the initiation of micro-pores will reduce the binding force between the matrix, resulting in a decrease in dynamic strength. Secondly, with the increase in impact times or strain, micro-pores gradually expand and penetrate each other, forming macroscopic cracks and accelerating the overall damage and failure of the sample.

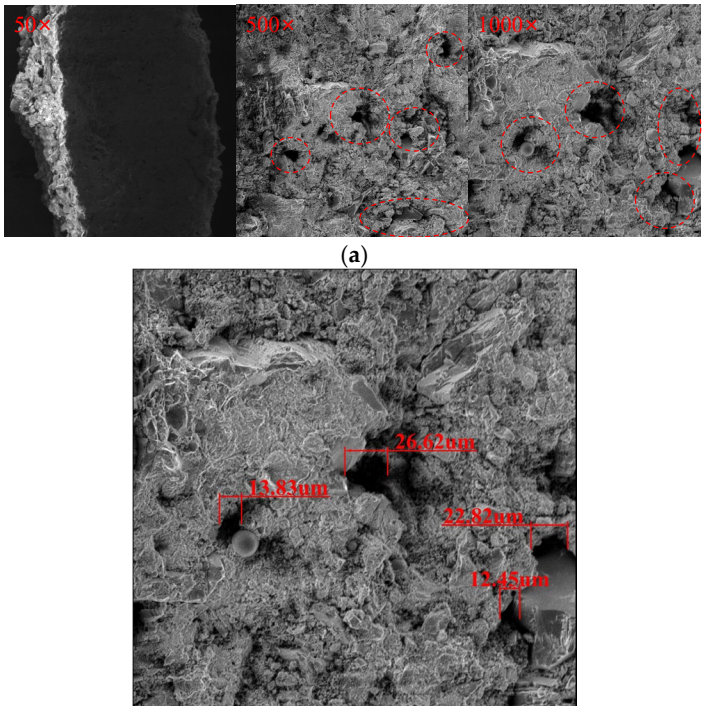


Figure 8. SEM pictures of 0.3 MPa nano-grouting material in the fracture (**a**,**b**).

Therefore, nano-grouting material is suitable for small engineering disturbances but not for large engineering disturbances. For example, it is an effective method to reinforce fractured rock mass by using nano-grouting material in shield construction.

Moreover, due to the small particles, nano-material can form dense structures (the denser the structure, the higher its brittleness) under higher pressure. However, the high brittleness of nano-material leads to the easy occurrence of micro-cracks under the dynamic impact of relatively high pressure (high strain rate) (the SEM pores in Figure 8 also verify this explanation to a certain extent), which reduces the dynamic strength. Superfine cement can enhance energy absorption through effective pulping structure and bonding properties and exhibit a stronger strain rate strengthening effect at a higher strain rate of SHPB. Moreover, the high specific surface area of nano-material is easy to cause local stress concentration, and the bond with rock is not tight, while the late strength of superfine cement increases steadily, and the toughness advantage of hydration products is more significant under higher impact pressure.

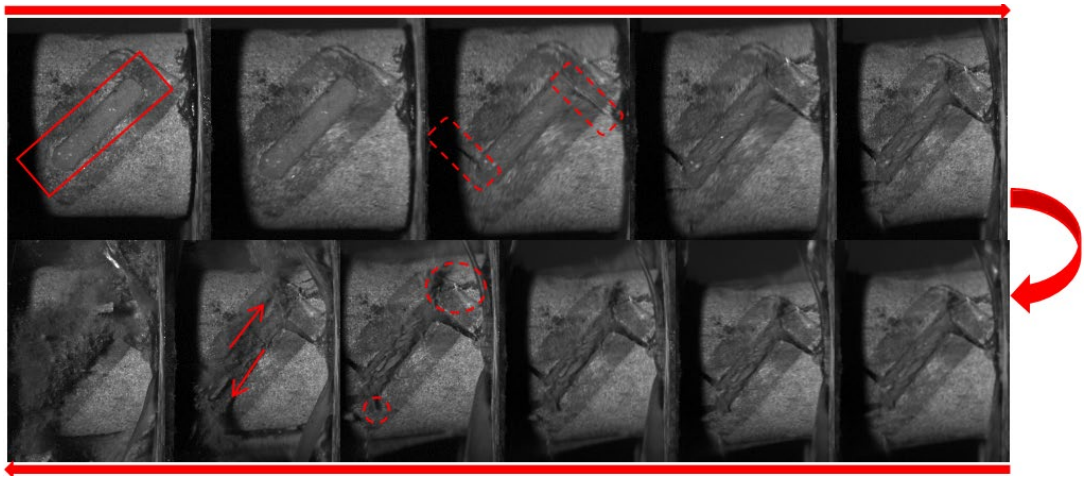
3.2. Macroscopic Dynamic Deformation and Failure Processes

In the literature, one study used a high-speed camera coupled with SHPB to record the progressive failure process of the grouted rock samples, and Digital Image Correlation (DIC) captured the strain evolution [26]. Another study in the literature obtained the

dynamic failure processes of the prefractured and grouted sandy mudstone specimens via a high-speed camera [35]. Based on these studies, we used the i-SPEED 508 high-speed camera to capture the whole process of dynamic failure of the grouted specimens, as shown in Figure 5b.

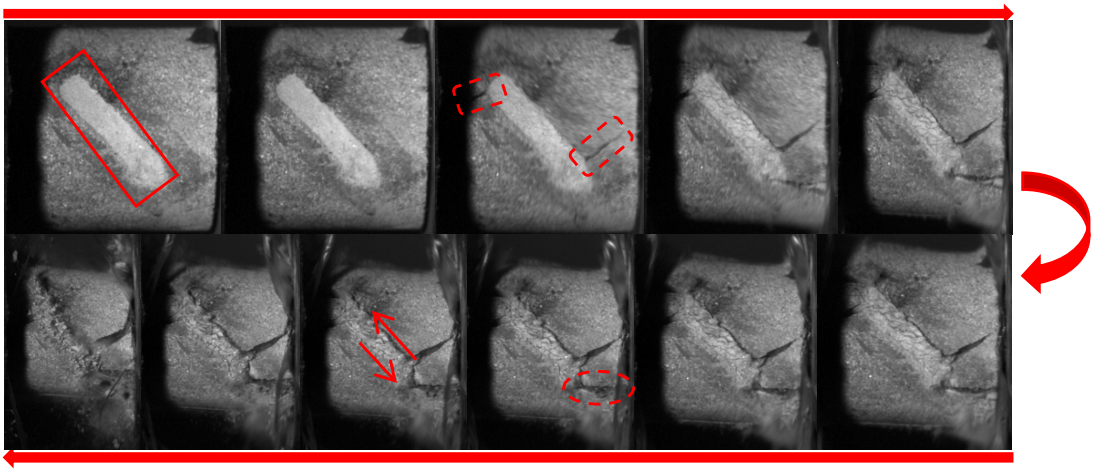
It can be seen from Figures 9 and 10, whether it be the nano- or the superfine cement grouting material, the impact fractures first occur at the two ends of the original grouted fracture and are the pair of parallel lines (dotted rectangles). According to the theory of elasticity, when there is fracture in rock specimen, the stress concentration phenomenon will occur at the tips of the fracture. During the impact loading process, the stress concentration factor at the tips of the original grouted fracture will increase significantly, which causes the two tips to reach their strength limits first; thus, the new fractures occur first at the tips. Moreover, the two tips of the original grouted fracture are relatively symmetrical, so the stress distribution is also relatively symmetrical. Since the stress concentration situations generated by the stress wave at two tips of the original grouted fracture are similar, the driving forces (mainly the tensile stress or shear stress generated by stress concentration) that the new fractures are subjected to during the initial stage of their generation and expansion are symmetrical in terms of direction and magnitude. This symmetrical stress state promotes new fractures to expand along similar directions, thereby forming an approximately parallel state. As the impact continues, the above-mentioned fractures continue to expand. Subsequently, fractures with indefinite directions appear at the ends of the original grouted fractures and then expand (oval dotted line). Meanwhile, the rock specimen slides and deforms along the length direction of the original grouted fracture (opposite red arrows), generating larger fracture that connects and penetrate with the fractures at the fracture ends. Eventually, the specimen is completely damaged.

In addition, compared with the impact air pressure of 0.1 MPa, the impact pressure of 0.3 MPa is higher, which leads to more severe damage to the rock specimen. For example, the fracture width and damage degree of the specimen are significantly greater than those of the specimen impacted by 0.1 MPa. From the perspective of energy, when the impact pressure is 0.3 MPa, more energy acts on the rock specimen compared to when it is 0.1 MPa: according to the law of conservation of energy, more energy will be used to damage the internal structure of the specimen, mainly manifested as the further expansion and penetration of fractures. From the perspective of stress concentration, the impact pressure of 0.3 MPa will generate greater stress concentration inside the specimen, thereby resulting in more severe damage.



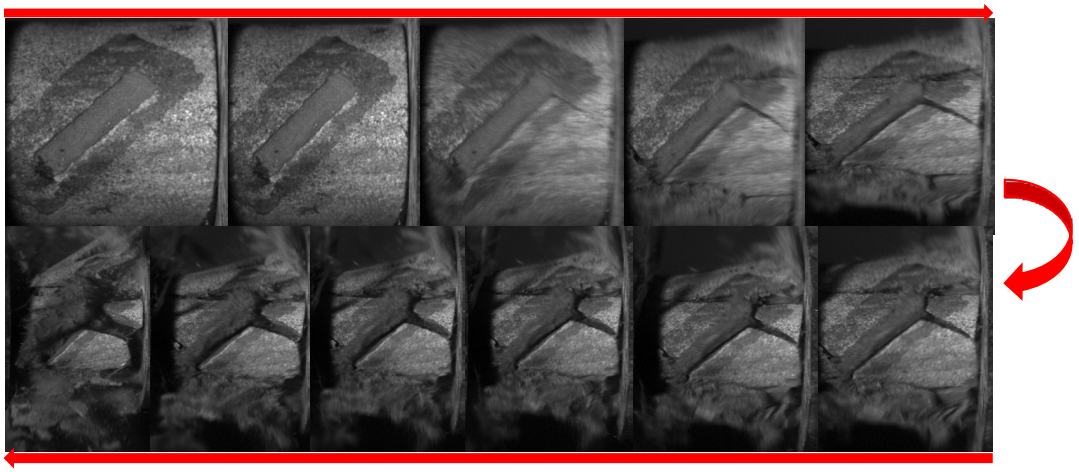
(**a**) Nano-grouted fractured rock

Figure 9. *Cont.*

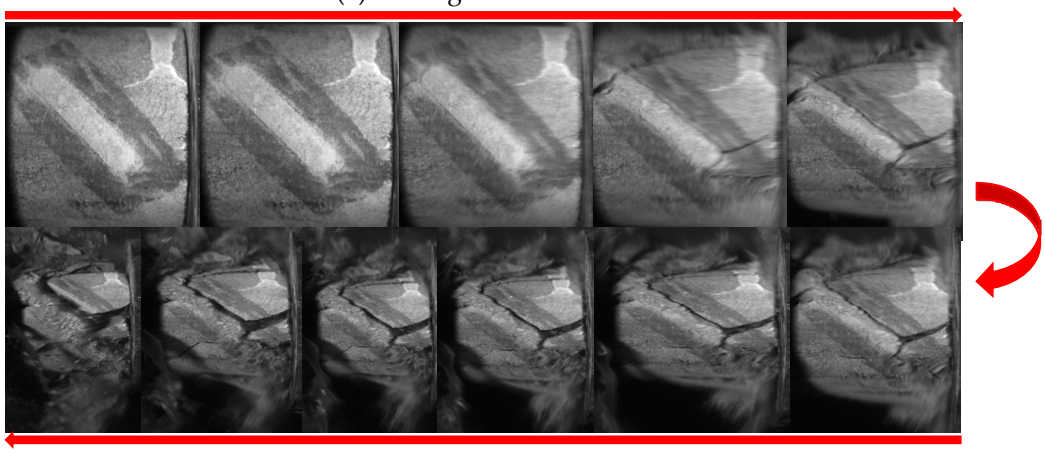


(**b**) Superfine cement grouted fractured rock

Figure 9. Dynamic deformation and failure processes of grouted fractured rock under impact air pressure of 0.1 MPa.



(**a**) Nano-grouted fractured rock



(**b**) Superfine cement grouted fractured rock

Figure 10. Dynamic deformation and failure processes of grouted fractured rock under impact air pressure of 0.3 MPa.

4. Conclusions

To enhance the stability of surrounding rock subjected to dynamic loading conditions, this study focuses on the development of innovative grouting materials and their rein-

forcement mechanisms. Utilizing the SHPB experimental setup, the dynamic mechanical properties and failure modes of grouted fractured rock based on nano-grouting material were systematically analyzed. Concurrently, high-speed imaging technology was employed to capture the macroscopic deformation and fracture propagation processes in real time, providing visual insights into the dynamic failure evolution. The main conclusions are as follows:

(1) The mechanical properties of nano-grouted fractured rock are better than those of traditional cement-based grouted rock under relatively low impact air pressure (0.1 MPa), with its dynamic peak strength increasing by 62.15%. However, when the impact air pressure is higher (0.3 MPa), the superiority of nano-grouting material decreases, with its dynamic peak strength decreasing by 56.24%, the possible cause of which is explained from the microscopic point of view, such as the formation of microscopic pores.

(2) The impact fractures first occur at the two ends of the original grouted fracture and are the pair of parallel lines, whether it be the nano- or superfine cement grouting material. Compared to 0.1 MPa, the impact pressure of 0.3 MPa causes more severe damage to the rock specimen.

(3) The nano-grouting material developed in this study can improve the dynamic mechanical properties and stability of rock under lower disturbance, which is suitable for low-disturbance engineering such as shield tunneling. However, under higher disturbances such as blasting, its strength decreases; so, it is necessary to improve the impact resistance in combination with bolt grouting support. In practical applications, materials should be selected according to their degree of engineering disturbance.

Author Contributions: Conceptualization, Y.J., S.Y. and P.H.; Methodology, Y.J., S.Y., H.G., L.H. (Lijun Han), P.H., M.C., H.S., L.H. (Lanying Huang) and S.S.; Validation, Y.J., S.Y., L.H. (Lijun Han), P.H., M.C., H.S., L.H. (Lanying Huang), S.S., S.W. and P.Q.; Formal analysis, Y.J., S.Y., L.H. (Lijun Han), P.H., M.C. and H.S.; Investigation, Y.J., S.Y., H.G., L.H. (Lijun Han), P.H., M.C., H.S., L.H. (Lanying Huang), S.S., S.W., P.Q. and X.B.; Resources, Y.J., S.Y., H.G., L.H. (Lijun Han), P.H., M.C., H.S., L.H. (Lanying Huang), S.S., S.W., P.Q. and Z.-a.L.; Data curation, Y.J., S.Y., H.G., L.H. (Lijun Han), P.H., M.C., H.S., L.H. (Lanying Huang), S.S., S.W., P.Q., X.B. and Z.-a.L.; Writing – original draft, Y.J., S.Y. and P.H.; Writing – review & editing, Y.J., S.Y., H.G., L.H. (Lijun Han) and P.H.; Visualization, Y.J., S.Y., H.G., L.H. (Lijun Han), P.H., M.C., H.S., L.H. (Lanying Huang), S.S., S.W., X.B. and Z.-a.L.; Supervision, Y.J., H.G., M.C., L.H. (Lanying Huang), S.S., S.W. and X.B.; Project administration, H.G.; Funding acquisition, Y.J., S.Y., P.Q. and Z.-a.L. All authors have read and agreed to the published version of the manuscript.

Funding: This research was financially supported by the Natural Science Foundation of Jiangsu Province (BK20220234, BK20230196, BK20240330), General Funded Project of China Postdoctoral Science Foundation (2023M733760), Natural Science Foundation of the Jiangsu Higher Education Institutions of China (21KJB580004, 22KJB130014), and Construction System Technology Project of Jiangsu Province (2023ZD033).

Data Availability Statement: The original contributions presented in this study are included in the article. Further inquiries can be directed to the corresponding author.

Conflicts of Interest: The authors declare no conflict of interest.

References

1. Shen, C.; Zeng, Z.; Lou, H.; Yang, Z.; Gu, W. Spatial deformation prediction method of fractured rock tunnel based on quantified GSI and its application. *Sci. Rep.* **2024**, *14*, 26088. [CrossRef] [PubMed]
2. Chen, M.; Zhang, Y.; Zhang, G.; Zhou, G.; Wang, Z. Discrete element study on mechanical response and pressure relief effect of rock containing variable hole. *Theor. Appl. Fract. Mech.* **2023**, *127*, 103976. [CrossRef]

3. Chen, M.; Zhang, Y.; Zang, C.; Zhang, G.; Li, Q.; Jiang, B. Experimental Investigation on Pressure Relief Mechanism of Specimens with Prefabricated Reaming Boreholes. *Rock. Mech. Rock. Eng.* **2023**, *56*, 2949–2966. [CrossRef]
4. Wang, W.; Feng, X.; Wang, Q.; Kong, R.; Yang, C. 3D DEM simulation of hard rock fracture in deep tunnel excavation induced by changes in principal stress magnitude and orientation. *J. Rock. Mech. Geotech. Eng.* **2024**, *16*, 3870–3884. [CrossRef]
5. Li, Y.; Xu, Z.; Pan, D.; Mou, W.; Zhao, S. A spatio-temporal forecasting method of fracture distribution using dynamically exposed rock images in tunnel: Methodology and application. *Eng. Geol.* **2024**, *343*, 107797. [CrossRef]
6. Shuang, H.; Liu, X.; Zhou, B.; Cheng, L.; Lin, H.; Hu, B.; Liu, Z. Study on the Energy Evolution and Damage Mechanism of Fractured Rock Mass Under Stress-Seepage Coupling. *Processes* **2025**, *13*, 270. [CrossRef]
7. Li, H.; Bai, H.; Xu, W.; Li, B.; Qiu, P.; Liu, R. Study on the Damage Evolution and Failure Mechanism of Floor Strata under Coupled Static-Dynamic Loading Disturbance. *Processes* **2024**, *12*, 1513. [CrossRef]
8. Chen, M.; Yang, S.; Ranjith, P.G.; Zhang, Y. Cracking behavior of rock containing non-persistent joints with various joints inclinations. *Theor. Appl. Fract. Mech.* **2020**, *109*, 102701. [CrossRef]
9. Chen, M.; Zang, C.; Ding, Z.W.; Zhou, G.L.; Jiang, B.Y.; Zhang, G.C.; Zhang, C.P. Effects of confining pressure on deformation failure behavior of jointed rock. *J. Cent. South. Univ.* **2022**, *29*, 1305–1319. [CrossRef]
10. Zhu, H.; Ju, M.; Cao, A.; Yu, L.; Cai, W.; Dou, L. Unloading-induced acoustic and fracturing behavior of a fault interface at various depths: Relevance to faulting-affected coal burst in deep mining. *Bull. Eng. Geol. Environ.* **2025**, *84*, 7. [CrossRef]
11. Wu, J.; Jing, H.; Yin, Q.; Yu, L.; Meng, B.; Li, S. Strength prediction model considering material, ultrasonic and stress of cemented waste rock backfill for recycling gangue. *J. Clean. Prod.* **2020**, *276*, 123189. [CrossRef]
12. Wu, J.; Wong, H.S.; Zhang, H.; Yin, Q.; Jing, H.; Ma, D. Improvement of cemented rockfill by premixing low-alkalinity activator and fly ash for recycling gangue and partially replacing cement. *Cem. Concr. Compos.* **2024**, *145*, 105345. [CrossRef]
13. Jin, Y.; Han, L.; Guo, H.; Yang, S.; Su, S.; Liu, Z.; Wang, S. Mechanical and macro-microscopic failure characteristics of grouted mudstone considering grout dehydration effect. *Eng. Fail. Anal.* **2022**, *142*, 106662. [CrossRef]
14. Shao, C.; Zhu, G.; Zhang, Q.; Duan, S.; Liu, R. Experimental study on sealing effect of cement-sodium silicate slurry in rock fracture with flowing seawater. *Tunn. Undergr. Space Technol.* **2025**, *155*, 106173. [CrossRef]
15. Guo, T.; Li, S.; Lu, B.; Wang, Z.; Cao, W.; Liu, S. Research on gradual optimization of slurry mixture ratio for shield tunnel backfill grouting based on fuzzy mathematics. *Constr. Build. Mater.* **2024**, *456*, 139319. [CrossRef]
16. Liu, L.; Wang, X.; Pi, J.; Cao, R.; Duan, Q.; Zhang, Q. Rock Mass Behavior During High Pressure Grouting: An In-Situ Experimental Investigation. *Rock. Mech. Rock. Eng.* **2024**, *58*, 2531–2547. [CrossRef]
17. Yu, X. Preparation and structure analysis of aluminum oxide/water glass/polyurethane composite grouting material for mining. *J. Build. Eng.* **2023**, *76*, 107170. [CrossRef]
18. Huang, S.; Zhao, G.; Meng, X.; Cheng, X.; Gu, Q.; Liu, G.; Zhu, S. Development of Cement-Based Grouting Material for Reinforcing Narrow Coal Pillars and Engineering Applications. *Processes* **2022**, *10*, 2292. [CrossRef]
19. Gao, X.; Wang, X.; Liu, X. New Chemical Grouting Materials and Rapid Construction Technology for Inclined Shaft Penetrating Drift-Sand Layer in Coal Mine. *Adv. Mater. Sci. Eng.* **2018**, *2018*, 2797419. [CrossRef]
20. Jiang, B.; Wu, M.; Wu, S.; Zheng, A.; He, S. A Review on Development of Industrial Solid Waste in Tunnel Grouting Materials: Feasibility, Performance, and Prospects. *Materials* **2023**, *16*, 6848. [CrossRef]
21. Zheng, M.; Li, S.; Lu, Y.; Lu, X.; Liu, L. The Performance Analysis of Grouting Repair Effect on the Accuracy of Disturbance Stress Test in Damaged Surrounding Rock Mass. *Materials* **2024**, *17*, 1926. [CrossRef] [PubMed]
22. Jin, Y.; Han, L.; Meng, Q.; Ma, D.; Wen, S.; Wang, S. Experimental investigation of the mechanical behaviors of grouted crushed coal rocks under uniaxial compression. *Geomech. Eng.* **2018**, *16*, 273–284.
23. Le, H.; Weng, M.; Li, H.; Li, J. Evaluating the Effect of Grouting on the Strength of Foliation of Metamorphic Rocks. *Rock. Mech. Rock. Eng.* **2024**, *57*, 2061–2079. [CrossRef]
24. Wu, D.; Zhou, L.; Nie, F.; Dai, F.; Wang, M.; Liu, B. Experimental and numerical investigation on the failure behavior of far-field-crack- tunnel rock mass under dynamic loads. *Tunn. Undergr. Space Technol.* **2025**, *156*, 106225. [CrossRef]
25. Xu, W.; Wu, H.; Lin, X.; Xie, Y.M. Numerical simulation and comparative design of non-planar interlocking fibre reinforced concrete bricks for tunnel lining structure under impact loading. *Tunn. Undergr. Space Technol.* **2025**, *155*, 106184. [CrossRef]
26. Kumar, S.; Tiwari, G.; Das, A. Dynamic Behavior of Ungrouted and Grouted Rocks of Different Morphologies Containing a Flaw Subjected to Different Thermal Treatments. *Rock. Mech. Rock. Eng.* **2024**, *57*, 261–286. [CrossRef]
27. Kumar, S.; Tiwari, G.; Parameswaran, V.; Das, A. Dynamic mechanical behaviour of rock -like materials with a flaw under different orientation and infill conditions. *Bull. Eng. Geol. Environ.* **2023**, *82*, 345. [CrossRef]
28. Gao, W.; Qin, S.; Li, K.; Wu, M.; Yang, M.; Shao, H. Microstructure manipulation in conductive polyethersulfone composite membranes: Impacts of carbon nanotube surface groups on its dispersion and segregation in membrane formation. *Sep. Purif. Technol.* **2025**, *359*, 130857. [CrossRef]

29. Chen, Z.; Zhang, X.; Shen, Y.; Geng, W.; Gong, C.; Zhang, Y.; Wang, G. Boosting ion uptake and electron transport through bridging Na2MnSiO4 with acidified carbon nanotubes for enhanced hybrid capacitance deionization. *Sep. Purif. Technol.* **2025**, *359*, 130429. [CrossRef]
30. Wang, X.; Wang, G.; Gao, Y.; Dong, X.; Zhang, X. Electro-assisted carbon nanotube dual catalytic membrane system for high-efficiency and energy-efficient water treatment. *Sep. Purif. Technol.* **2025**, *358*, 130406. [CrossRef]
31. Guo, F.; Xie, Z.; Zhang, N.; Zhang, C.; Guo, H.; Cui, G.; Xiang, Z. Study on the Pore-throat structure characterization and nano grouting law of the Low-permeability mudstone based on NMR-RSM methods. *Constr. Build. Mater.* **2022**, *342*, 127913. [CrossRef]
32. Wu, J.; Jing, H.; Gao, Y.; Meng, Q.; Yin, Q.; Du, Y. Effects of carbon nanotube dosage and aggregate size distribution on mechanical property and microstructure of cemented rockfill. *Cem. Concr. Compos.* **2022**, *127*, 104408. [CrossRef]
33. Xiang, Z.; Zhang, N.; Pan, D.; Xie, Z.; Wang, P.; Liang, D. Macroscopic and microscopic characteristics of nanosilica sol-based composite grout in sealing fractured argillaceous rock: A comparative study with silica sol and cement slurry. *J. Mater. Res. Technol.* **2025**, *34*, 898–911. [CrossRef]
34. Zhang, J.; Li, K.; Li, Y.; Liu, C.; Xu, J.; He, J. Applying Novel Micro-Nano-Siliceous Grouting Material Improves Mechanical Behaviors of Fractured Rock Masses and Microscopic Characteristics of Slurry-Rock Interface: Experimental and Numerical Simulation Investigations. *Rock. Mech. Rock. Eng.* **2024**, *57*, 8297–8321. [CrossRef]
35. Kao, S.; Zhao, G.; Meng, X.; Li, Y.; Liu, Z.; Zhang, R.; Huang, S. Dynamic Mechanical Characteristics of Fractured Rock Reinforced by Different Grouts. *Adv. Civ. Eng.* **2021**, *2021*, 8897537. [CrossRef]

Disclaimer/Publisher's Note: The statements, opinions and data contained in all publications are solely those of the individual author(s) and contributor(s) and not of MDPI and/or the editor(s). MDPI and/or the editor(s) disclaim responsibility for any injury to people or property resulting from any ideas, methods, instructions or products referred to in the content.